ELECTRONIC SUPPLEMENTARY INFORMATION

Pervasive infiltration and multi-branch chemisorption of N-719 molecules into newly-designed spongy TiO_2 layers deposited by gig-lox sputtering processes

Salvatore Sanzaro,[a,b] Enza Fazio,[a] Fortunato Neri,[a,**] Emanuele Smecca,[b] Corrado Bongiorno,[b] Giovanni Mannino,[b] Rosaria Anna Puglisi,[b] Antonino La Magna[b] and Alessandra Alberti[b,*]

[a] Department of Mathematical and Computational Sciences, Physics and Earth Sciences, University of Messina, Viale F. Stagno d'Alcontres 31, Messina 98166, Italy.

[b] National Research Council-Institute for Microelectronics and Microsystems (CNR-IMM), Zona Industriale - Strada VIII n°5, Catania 95121, Italy.

*alessandra.alberti@imm.cnr.it;

**fneri@unime.it

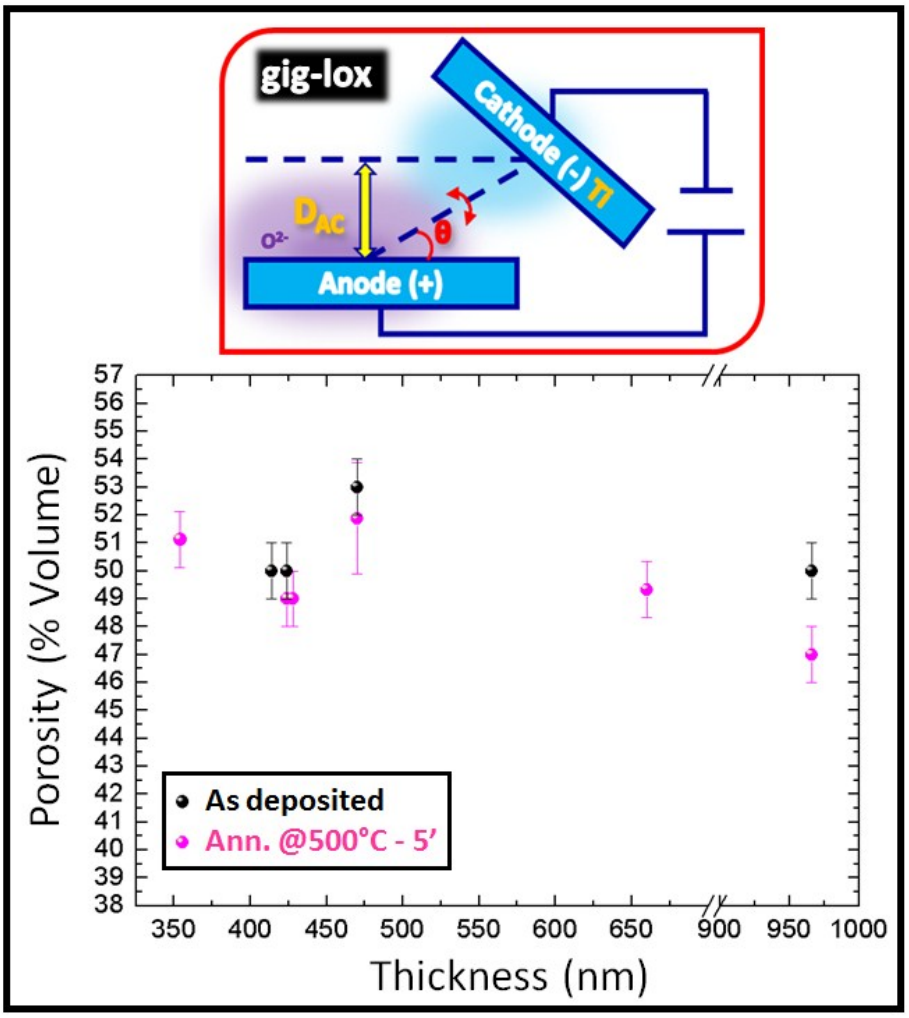

Fig. S1 Porosity trend as a function of thickness of TiO_2 layers deposited in gig-lox condition (see sketch)— before and — after annealing at 500°C for 5 minutes in air.

Micro-Raman analysis @532 nm

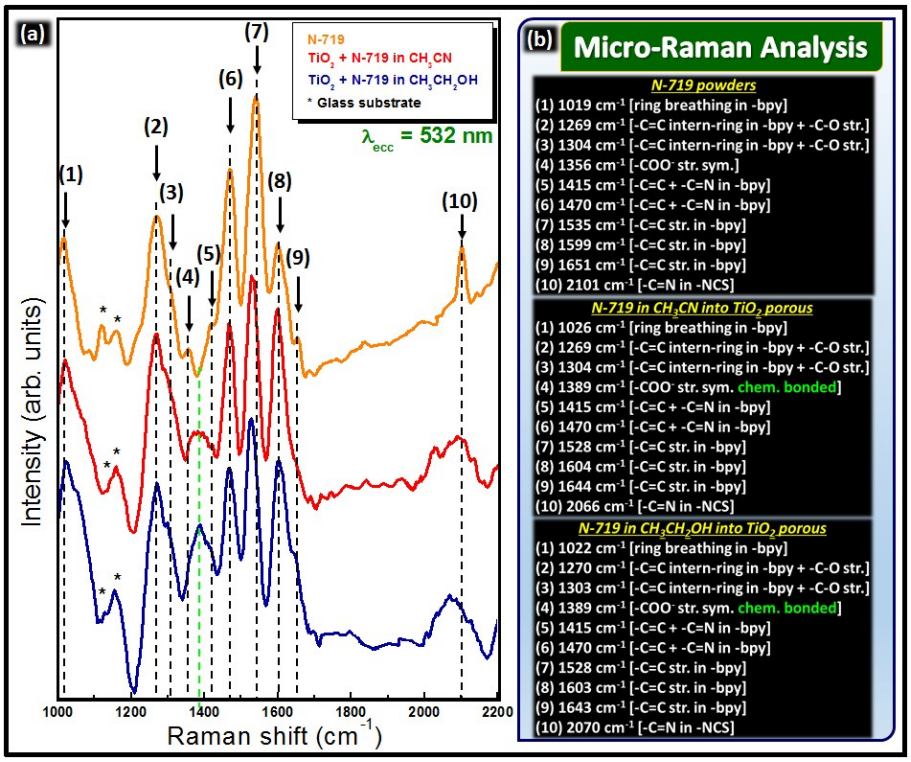

Fig. S2: Micro-Raman spectra of (a) — N-719, TiO_2 functionalized with N-719 in — CH_3CN or — CH_3CH_2OH; (b) list of the Raman vibrational modes in the N-719 powder or infiltrated into the TiO_2 layer (the scaffold).

ATR-FTIR analysis

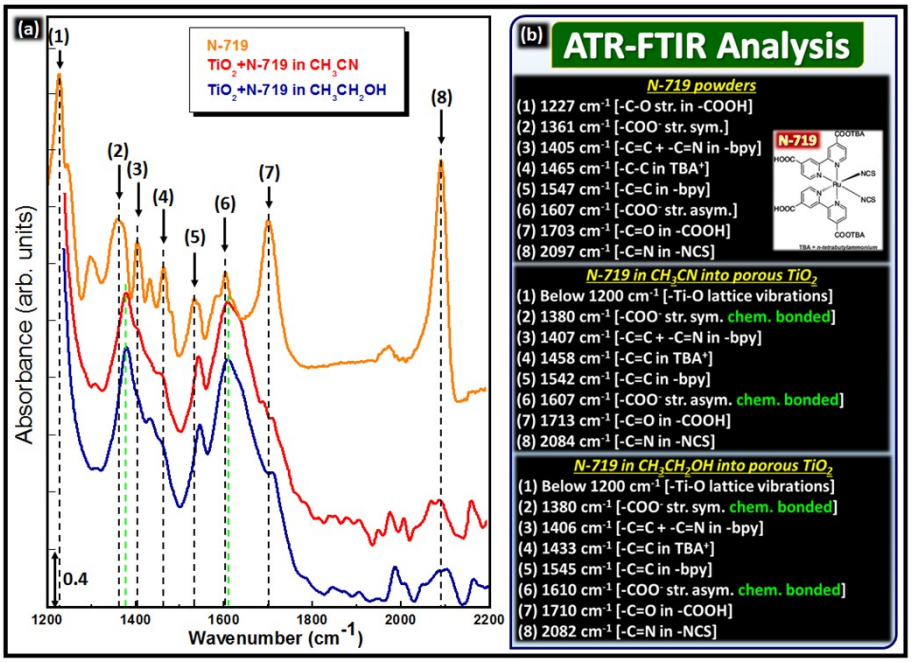

Fig. S3 ATR-FTIR absorbance spectra of (a) — N-719 powders, TiO_2 functionalized with N-719 in — CH_3CN or — in CH_3CH_2OH; (b) list of the Infra-Red vibrational modes in the N-719 powder or infiltrated into the TiO_2 layer (the scaffold).

XPS analysis

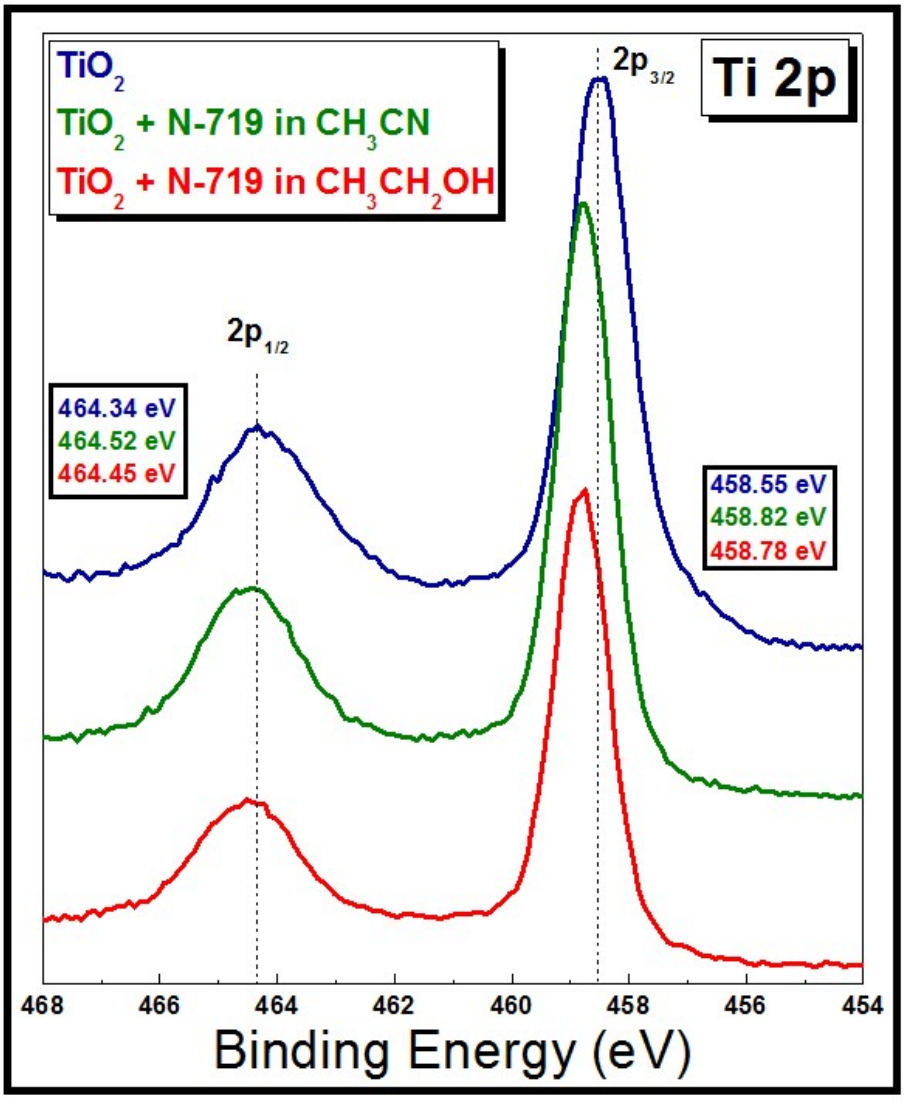

Fig. S4: HR-XPS spectra of — TiO_2 gig-lox annealed at 500°C, TiO_2 gig-lox annealed at 500°C sensitized with N-719 in —CH_3CN or — in CH_3CH_2OH.

Table S1 Ratio between the area of C and oxidized C peaks, area of carboxylate and carboxylic acid groups and average FWHM from the deconvolution.

Samples	Area C/Cox	Area COO-/COOH	Average FWHM
N-719 Powders	**10.93**	**1.57 ± 0.2**	**1.56**
TiO_2 + N-719 in CH_3CN	**12.95**	**3.50 ± 0.2**	**1.58**
TiO_2 + N-719 in CH_3CH_2OH	**15.04**	**2.34 ± 0.2**	**1.57**

Through the ratios between the area of carbon (-C-N, -C-C and –C-H) and oxidized carbon (-COOH and $-COO^-$) we found that, after functionalization, in the samples persists a little part of the solvent probably because this substitutes a ligand in the molecular structure.

Photocurrent measurements

To evaluate the molecular adsorption efficiency, one has to combine: 1) the layer porosity; 2) the full accessibility of the pores both inside the rods and downwards through the whole layer thickness. The two parameters reflect on the photo-carrier injection into the TiO_2 scaffold. The first point is given in Fig. S5a that provides us with the information on a slight variation of the porosity vs. thickness (it is reasonable to realize that thicker layers loses a bit of porosity, the error bars being considered). To be noticed that the porosity is an overall number including the nano and the meso pores in the count. The second point is elucidated by Fig. S5b wherein we show the density of molecules per unit area such to take into account the thickness of the layer (integrated surface density). This choice highlights that, being the surface density increasing with the TiO_2 thickness, thicker layers are able to host more molecules inside. The data at 330nm is (positively) out-of-trend due to the dominant percentage of nano-pores with respect to the total porosity for the first hundreds of nanometers. Consistently with those findings, in Fig. S5b we also show some conductivity data vs. the thickness, that measure the photo-carriers injection and collection capabilities by the TiO_2 scaffold (see paper for details). The cross correlation between the data, at the end, tell us that the higher the integrated surface density of the dye molecules (integrated over the thickness, namely the amount of dye molecules introduced into the scaffold), the higher the injection and collection of photo-electrons. Following the trend in figure S5b, it can be reasonably prospected that thick layers can have high adsorption efficiency and therefore high photo-carrier injection capability. The projection is consistent with the mainstays of the proposed growth method since it preserves the double-scale porosity of the layer (inter-rods (meso) and intra-rods (nano) porosity) during the bottom-up growth process. A complete device is given in our previous paper (Sci. Rep., 2016, 6, 39509), wherein we exploited a scaffold thickness of 1micron and a scattering layer to increase the photons capture efficiency. The solar cell efficiency was 6.3%.

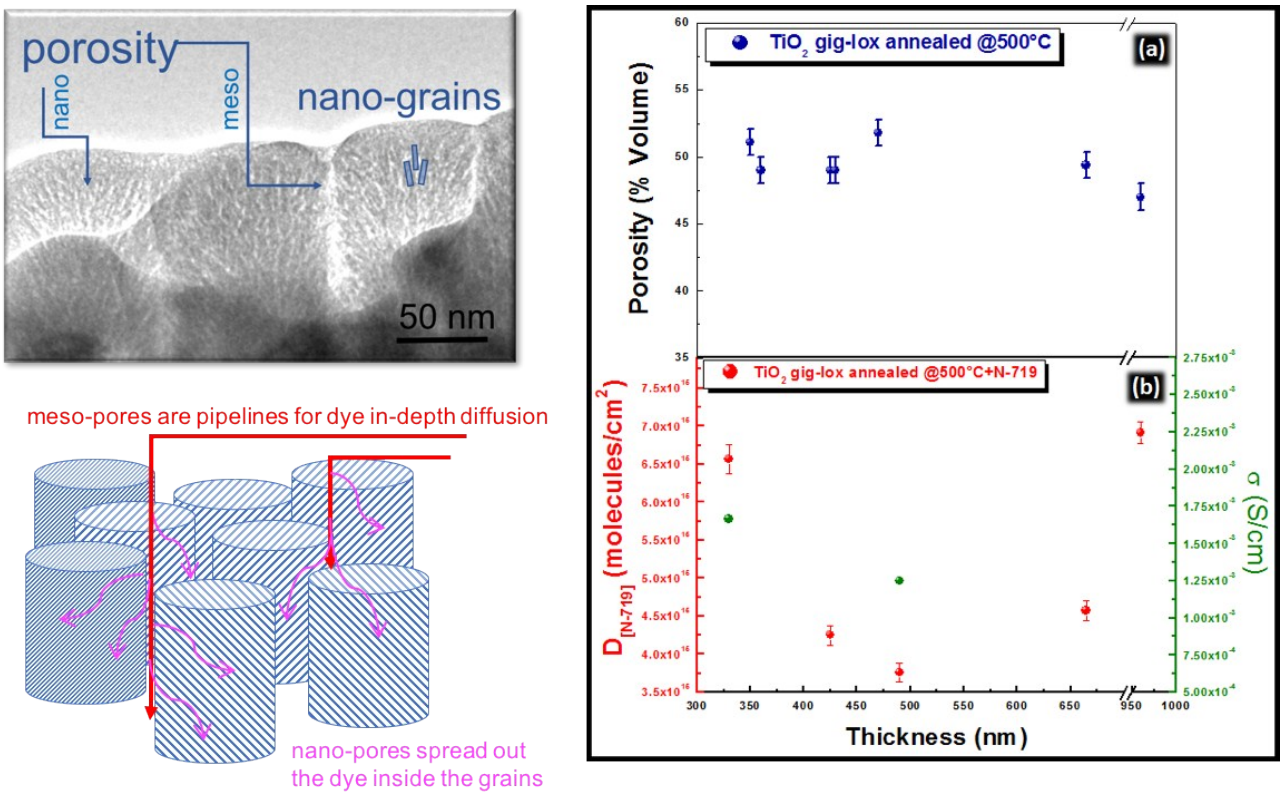

Fig. S5. Left panel: meso- and nano-porosity in a cross section of the sample and represented in a schematic to show the role of the mesopores as pipelines for in-depth dye diffusion. Through them, the dye molecules are spread out inside the network of intra-rods nano-pores. Right panel: cross-correlated density of dyes per unit surface (integral number of molecules in a given thickness) with the layer conductivity as a function of the layer thickness and in relationship with the overall layer porosity. The higher the amount of infiltrated molecules, the higher the photo-conductivity. The porosity data, being independent of the grown TiO_2 thickness, highlight that the structure of the layer is maintained during growth: this represent a main point of the gig-lox method

The effect of heating during irradiation is further evaluated in Fig. S5 by photocurrent measurements, with particular regards to the partial recovery of the layer conductivity through a cooling process (air blow).

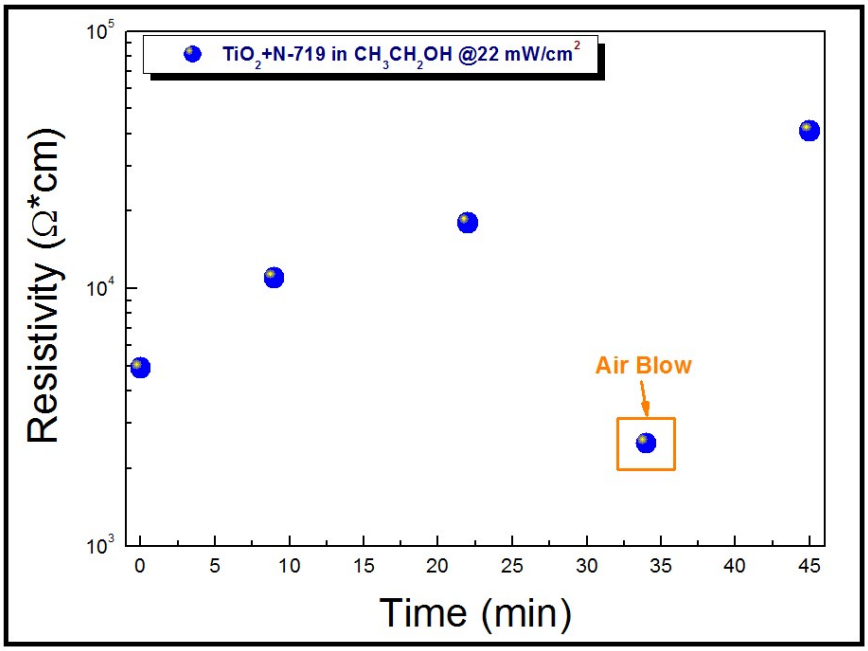

Fig. S6 Photocurrent data of TiO_2 functionalized with N-719 molecules ($1.01x10^{20}$ molecules/cm^3) in CH_3CH_2OH @22mW/cm^2. Where not written, the data are collected without air blow.

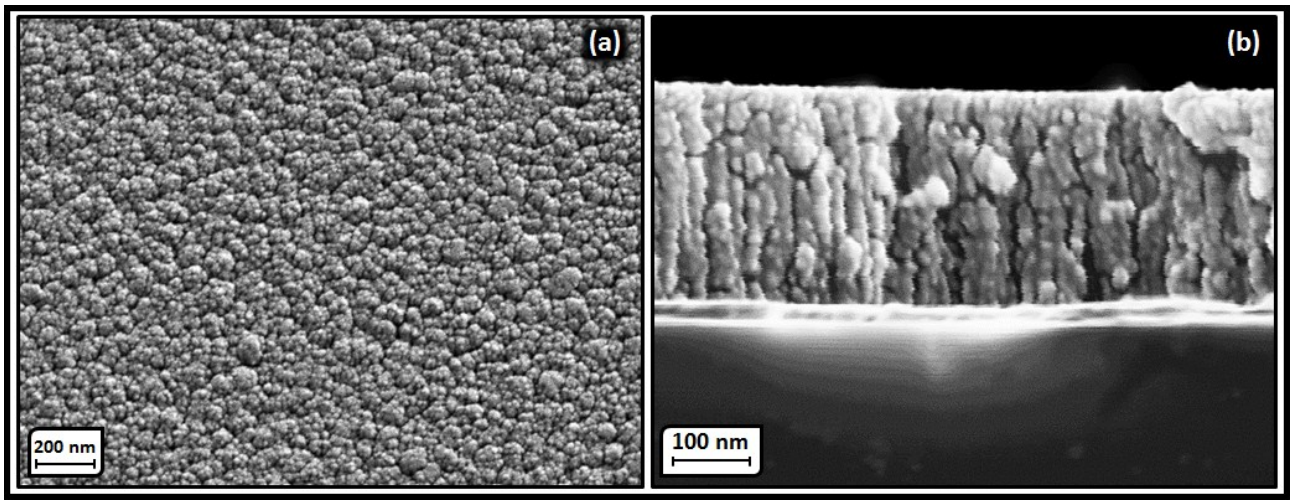

Fig. S7: (a) plan-view and (b) cross-section SEM images of gig-lox deposited TiO_2 layers to show the porous structure as a result of the bottom-up growth process.